Mortars with alkali-activated municipal solid waste incinerator bottom ash and fine recycled aggregates

S. Casanova[1], R. V. Silva[2*], J. de Brito[3], M. F. C. Pereira[4]

1 Instituto Superior Técnico, Universidade de Lisboa, Av. Rovisco Pais, 1049-001 Lisboa, Portugal (e-mail: sofia3casanova@gmail.com)
2 CERIS, Instituto Superior Técnico, Universidade de Lisboa, Av. Rovisco Pais, 1049-001 Lisboa, Portugal (*Corresponding author e-mail: rui.v.silva@tecnico.ulisboa.pt)
3 CERIS, Instituto Superior Técnico, Universidade de Lisboa, Av. Rovisco Pais, 1049-001 Lisboa, Portugal (e-mail: jb@civil.ist.utl.pt)
4 CERENA, Instituto Superior Técnico, Universidade de Lisboa, Av. Rovisco Pais, 1049-001 Lisboa, Portugal (e-mail: mfcp@ist.utl.pt)

Abstract: Milled municipal solid waste incinerator bottom ash was used as a precursor in the production of alkali-activated mortars with recycled concrete aggregates as a sand substitute. Fly ash was used as control precursor and sodium hydroxide as an alkaline activator. Different thermal curing regimens were used: 24 h in ambient conditions; 24 h/70 °C; 48 h/70 °C; and 24 h/90 °C. Mechanical and durability-related performances were evaluated (i.e. flexural and compressive strength, modulus of elasticity, ultrasonic pulse velocity, carbonation, capillary water absorption, and shrinkage). The reaction between metallic aluminium from municipal solid waste incinerator bottom ash and OH^- ions produced hydrogen gas, causing expansion, porosity increase and thus decline in performance. Low stability in high relative humidity settings due to leaching of highly soluble compounds was also observed. A further decline in performance was observed in mixes containing recycled aggregates. Alkali activated municipal solid waste incinerator bottom ash presented fast carbonation but also a considerable strength enhancement.

Keywords: municipal solid waste; incinerator bottom ash; alkali-activated materials; recycled aggregates; curing conditions.

Declarations of interest: none

1 Introduction

Alkali-activated materials (AAM), which have been regarded as one of the best alternatives to cement in concrete and mortar production, are the product of a reaction between a solid aluminosilicate (i.e. precursor) in an alkaline medium (i.e. alkali activator) (Provis, 2018). The solid precursor usually consists of aluminosilicate supplementary cementitious materials, including ground granulated blast furnace slag (GGBS), coal fly ash (FA), calcined clays and natural pozzolans, having demonstrated good results (Provis and van Deventer, 2014). Geopolymers, which share the concept of production with AAM (i.e. dissolution of the precursors' amorphous phases using a strongly alkaline solution), though exhibiting polymeric systems and mechanical behaviour, have shown a considerable ability to immobilize heavy metals, fast setting at room temperature, high resistance to acid attack and high compressive strength (Davidovits, 1994). Furthermore, despite some variability in the values in the literature, life cycle assessments demonstrated 55-75% lower CO_2 emissions when compared to equivalent cement-based materials (Yang et al., 2013).

Since there has been a shift towards renewable sources, the generation of FA has been declining, which will naturally affect potential supply chains for AAM based on FA (Rowlatt, 2019). Additionally, though the production of new steel relies on blast furnaces, metal recycling in electric arc furnaces is preferred due to their higher efficiency, thereby decreasing GGBS production (Singh, 2012; Zhong, 2018). For this reason, there is considerable scope in studying other solid precursors for AAM production.

In Europe, about 20 million tonnes of MSW are produced each year (Nørgaard et al., 2019). The incineration of this waste results in two by-products - fly ash and bottom ash. The former is generally comprised of hazardous compounds and must be treated before their application or safe disposal (Ferraro et al., 2019). The incinerator bottom ash from MSW (MIBA) represents 85-95% of the incineration products (Dhir et al., 2018). It is a highly siliceous by-product, with a

notable amount of calcium-based phases as well as alumina and iron oxides (Kurda et al., 2020), capable of being valorised in the production of AAM, which can therefore reduce its landfilling (Silva et al., 2017). The existing studies on the alkali activation of MIBA show that it is reactive to the presence of a strongly alkaline medium, though not without its limitations. In the study of Chen et al. (2016), wherein alkali-activated MIBA was used to produce aerated specimens, alkaline solutions with different concentrations of NaOH were used (2 M, 4 M, 8M and 12 M). The authors adopted different mix durations, ranging from 15 to 120 min, to potentiate the corrosion of metallic Al, which is present in a relatively great amount in MIBA. This corrosion is known to result in the production of H_2 gas, which is meant to be the aerating agent in this case. An alkaline solution with a concentration of 8 M and mixing time of 60 min revealed to optimal to enhance the mechanical performance and porosity.

In the study of Galiano et al. (2011), FA and MIBA were used as solid precursors (74% and 26%, by weight, respectively, of the total binder). Different contents of NaOH, KOH (~4% by weight of the precursors), Na_2SiO_3 and K_2SiO_3 (~21% by weight of the precursors) were used as activators. The specimens were cured in ambient conditions and at a temperature of 60 °C. Relatively low compressive strength was observed in all specimens regardless of the activator, with a maximum of 7 MPa and almost all below 1 MPa. Although it was not stated by the authors, this low performance was probably due to the formation of H_2 gas from the reaction of Al with the OH^--rich solution. Specimens cured at 60 °C exhibited higher strength than that of those cured at ambient temperature.

Cristelo et al. (2020) produced pastes using varying concentrations of NaOH (4-12 molal) in the alkaline activator as well as with the incorporation of sodium silicate (SiO_2/Na_2O weight ratio of 2.0) for the activation of MIBA and/or fly ash from MSW incineration. Liquid to solid ratios varied between 0.35 and 0.50. Compressive strength values of mixes with NaOH alone were low (between 1.5 MPa and 3 MPa) but increased with the use of sodium silicate (over 10 MPa). The

decline in performance was mostly due to the extensive expansion caused by the reaction of Al with the NaOH solution. When exposed to wetting and drying cycles, specimens with a 4 m NaOH activator exhibited quite low stability, demonstrating severe mass loss after each cycle.

Huang et al. (2018) assessed the influence of different curing methods on the performance of mortars containing alkali-activated 60 wt% MIBA and 40 wt% GGBS. The alkali activator was a combination of 4.8 M NaOH solution and Na_2SiO_3 with a modulus of 2.6 (weight proportions of the total solution of 55% and 44%, respectively). The methods consisted of natural curing (5-20 °C and 60% RH), standard curing room (20 ± 2 °C and > 95% RH), seal curing (20 ± 2 °C and > 95% RH), steam curing (80 ± 2 °C and > 100% RH) and soaking curing (20 ± 2 °C and 100% RH). 28-day compressive strength varied between 28 MPa and 53 MPa, depending on the curing method. The authors observed that natural and soaking curing methods yielded lower strength due to leaching of OH^-, which led to a reduction of pH and thus lower dissolution of active components. The optimum performance was observed in samples cured in high RH environment, yet with low contact with external water (i.e. seal and standard curing methods).

Huang et al. (2020) studied the effect of increasing NaOH content (1.7%, 5.6% and 11.1% by weight of total precursor) of mortars containing alkali-activated MIBA and GGBS. The sodium silicate solution (9.65% Na_2O, 25.22% SiO_2, and 65.13% H_2O) content was constant and about 27% of the binder's weight, to which water and NaOH were added. Increasing the amount of NaOH content led to higher pH levels, which translated into a more effective dissolution of aluminosilicate phases and thus improved strength development (47.4 MPa for mixes with NaOH content of 5.55% that of the weight of the precursors). 28-day compressive strength of 27.9 MPa and 36.5 MPa were observed for mixes containing about 2% and 11% of NaOH, respectively, indicating optimum levels in between. Through a conversion rule between free and "union" alkali, the authors demonstrated that, for a given amount of total alkali incorporated in the mortars, there was a considerable loss of alkali in mixes made with sodium silicate

alone to the external environment (diffusion mechanism to achieve equilibrium with an efflorescence phenomenon). The amount of "union" alkali, which corresponds to that of resulting from the polymerization process, was higher for mixes with a 5.55% NaOH content.

Atiş et al. (2015) analysed the influence of the curing conditions of AAM based on class F FA. All mixes were designed with an aggregate/FA ratio of 3 and water/FA ratio of 1/3. The authors stated that alkali activators with various concentrations of Na^+ (4% to 20% by weight of the precursor with 2% increment) from a 97% pure NaOH. The specimens tested had different combinations of curing temperatures (varying between 45 °C and 115 °C), ratios of Na^+/FA (4-20%) and curing time (24 h, 48 h, 72 h). Increasing the curing period from 24 h to 48 h led to a generalised strength increase, though equivalent results were observed by increasing up to 72 h. The optimum performance was observed in specimens cured in 115 ºC for 24 h, and with a Na^+/FA ratio of 14% (compressive and flexural strengths of 120 MPa and 15 MPa were, respectively, observed). No strength gain was observed for curing temperatures of 45 °C. On the other hand, in several cases of specimens cured at 115 °C, no strength gain was observed. This was attributed to fast evaporation of the solvent, which may have prevented the adequate dissolution of the FA's particles.

Fang et al. (2018) analysed the performance of FA/GGBS-based alkali-activated concrete cured at ambient temperature. GGBS content varied between 10% and 30% by weight of the total binder. The alkaline solution to binder ratio was set at 0.4 and the molarity of NaOH varied between 10 M and 12 M. The ratio between the Na_2SiO_3 and NaOH was kept constant at 2. All mixes presented setting at ambient conditions (initial and final setting times were found to be in the range of 80-350 min and 100-470 min, respectively). The incorporation of GGBS significantly reduced setting time. Specimens with 30% GGBS presented a higher strength gain over time, reaching 56 MPa after 28 days, whereas those with 10% GGBS and 90% FA showed a compressive strength of about 22 MPa, in the same period.

127 Regarding the effect of incorporating recycled aggregates (RA) in AAM, little research has
128 been carried out. In the study of Alonso et al. (2018), mortars were produced using RA from
129 crushed concrete and ceramic particles. The precursors for AAM were GGBS and FA, and
130 conventional mortars using cement were also produced. The activator for the GGBS mixes was
131 a sodium silicate and sodium hydroxide solution ($Na_2O \cdot nSiO_2 \cdot mH_2O$ + NaOH) with a
132 SiO_2/Na_2O ratio of 1.2 and 4% Na_2O by mass of the precursor. For FA mixes, the activator was
133 a 10 M NaOH solution plus 15% sodium silicate solution. GGBS- and FA-based mortars pre-
134 sented 28-day compressive strength values of about 91 MPa and 24 MPa, respectively, whereas
135 the control cement mortar showed a compressive strength of about 75 MPa. As expected, the
136 incorporation of RA led to a decline of mechanical performance. Regardless of the binder,
137 losses of 40-50% and 60-70% in the 28-day compressive strength were observed for mixes
138 with 100% RA from crushed concrete and ceramic bricks, respectively.

139 Nuaklong et al. (2016) evaluated the influence of coarse RA from crushed concrete in mixes with
140 alkali-activated FA. The activator was comprised of a fixed content of 162 kg/m^3 of aqueous
141 Na_2SiO_3 and 108 kg/m^3 of a NaOH solution with different concentrations (i.e. 8 M, 12 M and 16
142 M). Specimens were subjected to 60 °C curing temperature for 2 days and subsequently placed
143 in a controlled environment at 23 °C and 50% RA for 7 days. The compressive strength of control
144 specimens was marginally affected with varying concentration of the NaOH solution. However,
145 this parameter was more sensitive to the incorporation of RA; mixes with 8M, 12 M and 16 M
146 NaOH solutions showed compressive strength values of 30.6 MPa, 38.4 MPa and 34.8 MPa,
147 respectively (76%, 93% and 87%, respectively, when compared with the FA mixes).

148 This study is part of a state-funded research project in Portugal, connecting corporations within
149 the construction sector, intending to further reduce the environmental impact and cost associ-
150 ated with the production of structural concrete by means of the alkali activation of MIBA as

integral replacement of cement and RA as a substitute of sand. The purpose of this study was to evaluate the performance of alkali-activated mortars subjected to different curing conditions, with MIBA as the precursor to obtain a stable product with enough mechanical performance. The literature review shows that few studies were carried out on the influence of different curing regimens of MIBA-based AAM with none on MIBA as the sole precursor and that only one relevant study was made on AAM containing RA from construction and demolition waste. The behaviour of some of the mortars in this study is compared with that of cement mortars and alkali-activated mortars with FA as the precursor. X-ray fluorescence (XRF) and powder XRD analyses were carried out on cement, FA, MIBA and selected mortars. The specimens' mechanical and durability-related performances were evaluated through their flexural and compressive strength, ultrasonic pulse velocity, modulus of elasticity, carbonation, water absorption by capillary action, and shrinkage.

2 Materials and test methods

2.1 Cement and precursors

Cement CEM I 42.5R was used as the control for conventional mortars. The alkaline activator (AA) was a solution of water and NaOH (99% purity), with mass percentages of 71.4% and 28.6%, respectively (10 m NaOH solution). Class F coal FA (ASTM-C618, 2019), provided by the Portuguese cement producer Secil, was used as the control binder for AAM. MIBA was sourced from the Valorsul's MSW treatment plant, located in São João da Talha, in the municipality of Loures, Portugal. This waste-to-energy power plant is a moving grate furnace that treats undifferentiated waste from households in the Great Metropolitan Area of Lisbon. In mortars with MIBA, lignosulphonate-based water-reducing admixture was used (2% of Sikament 400 Plus by weight of binder). X-ray fluorescence (XRF) analysis was carried out on cement, MIBA and FA. For the first two, XRF analysis was made with a Niton XL3T GOLDD

spectrometer from Thermo Scientific with an X-ray generator of 50 kV/200 μA, equipped with a CCD for image location (3 mm spot diameter) and storage, whereas the latter's composition was obtained by wavelength dispersive XRF, using an S4 Pioneer apparatus of BRUKER, with a potential of 4 kV. Scanning electron microscopy (SEM), energy-dispersive X-ray spectroscopy (EDS), and quantification of magnetic metal and metallic aluminium fractions were carried out for additional characterization of MIBA. The fraction of metallic aluminium was quantified through the stoichiometry of the reaction of MIBA in a 2.5 M NaOH solution. The amount of H_2 gas released from this reaction was measured and compared with a control test comprising metallic Al alone. The pozzolanicity of MIBA and FA was quantified using the Chapelle test (Ferraz et al., 2015; NBR-15895, 2010). The water used in the production of all specimens was potable tap water complying with Directive 98/83/CE (CEU, 1998).

2.2 Aggregate and mortar test methods

The natural aggregates (NA) were siliceous fine and coarse sands (0/1 and 0/4, respectively), whereas the RA was sourced from crushed concrete produced at the Construction Laboratory at IST. At least three samples of each material/mortar mix were analysed for every test presented in this paper. The aggregates' particle size distribution test was carried out as per EN 1015-1 (EN-1015-1, 1999). The bulk density was tested according to EN 1097-3 (EN-1097-3, 1998), and water absorption and apparent densities with EN 1097-6 (EN-1097-5, 2008). The dynamic behaviour of water absorption by RA was evaluated by means of the test method presented in Rodrigues et al. (Rodrigues et al., 2013), to calculate the amount of compensating water. This method consists of measuring the water absorbed by fine RA over time in a hydrostatic scale using a sodium hexametaphosphate [$(NaPO_3)_6$] solution. This dispersant was used in this test method to prevent agglomeration of particles, which is a phenomenon that typically occurs during this test and that hinders the measurement of water absorption.

The production of mortar specimens was based on EN 1015-2 (EN-1015-2, 1999). The consistence of fresh mortars was evaluated as per EN 1015-3 (EN-1015-3, 1999). The performance of mortars in the hardened state was evaluated according to bulk density (EN 1015-6 (EN-1015-6, 1999)), dynamic Young's modulus (ASTM E1876 (ASTM-E1876, 2015)), ultrasonic pulse velocity (EN 12504-4 (EN-12504-4, 2004)), flexural and compressive strength (EN 1015-11 (EN-1015-11, 1999)), carbonation (LNEC E391 (LNEC-E391, 1993)), water absorption by capillary action (EN 1015-18 (EN-1015-18, 2002)), and shrinkage (EN 1015-13 (EN-1015-13, 1993)).

The mortars' constituents and the resulting specimens (dried and ground just after being tested) were analysed by means of XRD patterns using a Bruker D8 Discover A25 instrument with Cu-Kα radiation. Diffraction patterns were obtained by scanning the goniometer from 10° to 80° (2θ) at a rate of $0.05°{\cdot}s^{-1}$.

2.3 Mix design

The production of all mortars (total of 336 specimens with a standard size of 40 mm × 40 mm × 160 mm; 21 specimens per type of mix) followed the guidelines of EN 196-1 (EN-196-1, 2005), but for alkali-activated MIBA mortars, extended mixing time was required to potentiate corrosion of metallic aluminium (15 min mixing + 45 min resting before placing in the moulds vs. 4 min as expressed in EN-196-1 (2005)). Minimal loss of workability and no setting were observed during this extended mixing time thereby suggesting marginal precipitation of reaction products. A slight adaptation was also required for mixes with RA to allow the absorption of compensating water; RA were mixed with 2/3 of the total effective water for 5 min before adding the rest of the components. The method adopted for the mix design yields mortars exhibiting characteristics and performance equivalent to those of a concrete counterpart and not mortars typically used for rendering and masonry. All mortars have a volumetric proportion of binder/aggregates of 1/3. A liquid/binder ratio of 0.5 was used to compare mortars made with cement, FA and MIBA. A ratio

of 0.65 was applied to analyse MIBA mortars alone, with a variation of the RA fraction. Further explanation of this variation is in section 3.2.1.

Concerning the curing conditions, all specimens were cured for 24 h in the laboratory (sealed curing with plastic film around the moulds). After that, samples were cured in different environments: 24 hours in ambient conditions (~18 °C and RH of ~65%); 24 hours at 70 °C; 48 hours at 70 °C; and 24 hours at 90 °C. After the thermal curing, all specimens were stored in an environmental chamber with a constant temperature of 20 °C and RH of 60% until testing age (the total age of the specimens corresponds to the time from the moment of production until testing). Table 1 provides the mix code for the alkali-activated mortars; FA-NA and FA-RA correspond to alkali-activated FA mortars, whereas BA-NA and BA-RA are alkali-activated MIBA mortars. It should be noted that none of the MIBA-based mortars cured in ambient conditions exhibited setting after one week and thus could not be further characterized.

Table 1 - Mix code for alkali-activated mortars

Mix code	Binder	Aggregate	Curing
FA-NA 70/24	Fly ash	Natural aggregates	70 °C for 24 h
FA-NA 70/48			70 °C for 48 h
FA-NA 90/24			90 °C for 24 h
FA-RA 70/24		Recycled aggregates	70 °C for 24 h
FA-RA 70/48			70 °C for 48 h
FA-RA 90/24			90 °C for 24 h
BA-NA 70/24	Bottom ashes from MSW incineration	Natural aggregates	70 °C for 24 h
BA-NA 70/48			70 °C for 48 h
BA-NA 90/24			90 °C for 24 h
BA-RA 70/24		Recycled aggregates	70 °C for 24 h
BA-RA 70/48			70 °C for 48 h
BA-RA 90/24			90 °C for 24 h

3 Results and discussion

3.1 Material characterization

3.1.1 Cement and precursors

Table 2 presents the composition of the main oxides of the binders from the XRF analysis. The composition of FA is what one would expect from a Class F; the sum of Al_2O_3 + SiO_2 + Fe_2O_3

242 is equal to 84.8% and exceeds the minimum value established (i.e. 70% by weight) following
243 EN 450-1 (EN-450-1, 2012). The composition of MIBA shows lower content of Al_2O_3 and
244 Fe_2O_3 and a considerably larger fraction of CaO. According to ASTM C618, MIBA could be
245 classified as class C FA, wherein the minimum value of the sum of Al_2O_3, SiO_2 and Fe_2O_3 is
246 50 wt%. It has been shown that about 66% of the MIBAs in the literature satisfy this limit
247 (Lynn et al., 2017). An additional characterization based on the magnetic separation (using a
248 neodymium magnet) of a random sample of MIBA (24 g), showed that about 12% and 88%
249 were magnetic and non-magnetic residues, respectively. This shows that the electromagnetic
250 separation stage applied at the MIBA's treatment facility was not optimized and further quan-
251 tities of material could be recovered. Even though the quantification of amorphous Fe phases
252 was not carried out, a notable amount may be present considering the overall quantity of total
253 Fe-bearing phases. Future analysis will be carried out on this aspect since amorphous Fe phases
254 inhibit the dissolution of Si and Al phases (Chen-Tan et al., 2009), thus hindering the strength
255 development of the resulting mortars.

256 Table 2 - XRF of cement, FA and MIBA

Material		SiO_2 (%)	Al_2O_3 (%)	Fe_2O_3 (%)	CaO (%)	MgO (%)	SO_3 (%)	K_2O (%)	TiO_2 (%)	CuO (%)	Na_2O (%)	P_2O_5 (%)
Cement		19.49	5.02	3.32	63.48	1.26	3.26	-	-	-	-	-
FA		51.93	18.75	15.96	4.46	0.90	-	3.24	2.39	1.60	0.76	-
MIBA	Original	51.84	5.00	9.29	23.00	2.36	2.42	1.57	0.34	0.16	-	2.29
	Magnetic	14.92	4.71	62.61	9.86	2.57	1.36	0.48	0.58	0.15	-	1.26
	Non-magnetic	53.74	4.49	6.69	24.25	2.33	2.42	1.60	0.33	0.18	-	2.23

257

258 After ball mill processing (GEOLAB-IST), MIBA exhibited an average particle size under 45 μm.
259 The XRD analysis (Figure 1) of the milled MIBA showed that it contains some amorphous fraction
260 (broad reflexion peak between the 15º and 40º 2θ positions), which can be mostly attributed to the
261 waste glass fraction. This was confirmed by stereomicroscopic observations of the unprocessed
262 MIBA (Figure 2). The XRD spectrum primarily show quartz peaks (SiO_2 - International Centre for
263 Diffraction Data - ICDD # 33-1161). Other mineralogical phases included calcite ($CaCO_3$ - ICDD

264 # 05-0586), rutile (ICDD # 21-1276) and anorthite ([Ca, Na][Si, Al]$_4O_8$ - ICDD # 20-0020). XRD
265 analysis was also carried out on the two phases resulting from the magnetic separation stage. The
266 non-magnetic fraction showed main peaks of quartz, calcite and anorthite, whereas the magnetic
267 fraction showed peaks of magnetite (Fe_3O_4 - ICDD # 03-0863) and kamacite (Fe, Ni - ICDD # 37-
268 0474).

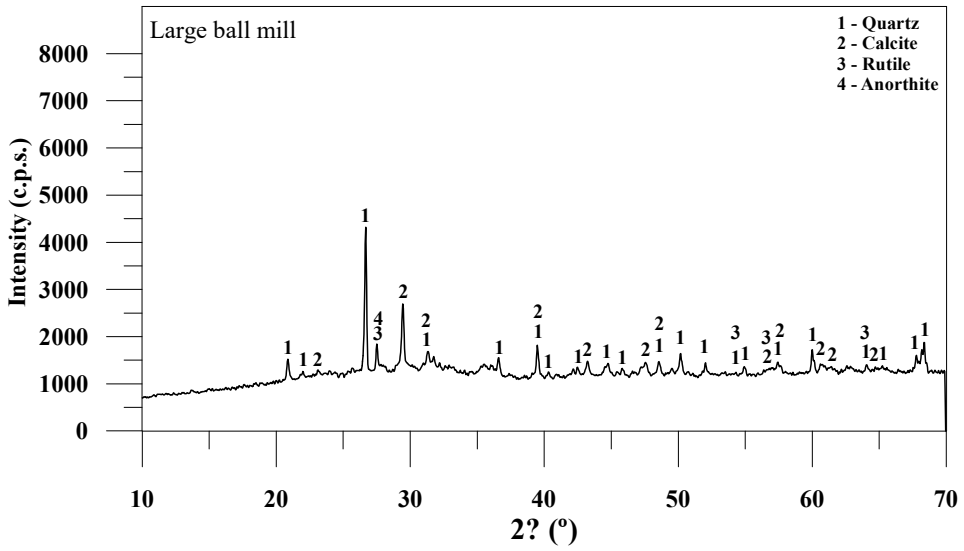

269

270 Figure 1 - XRD of MIBA processed in a large ball mill machine

271

272

273 Figure 2 - Stereomicroscopic image of a sample of washed MIBA

274

275 The morphology of MIBA can be seen in Figure 3a. The particles are irregular and have an
276 angular shape, which can affect the workability of mixes. The semi-quantitative EDS results
277 (Figure 3b), based on an elemental mapping of the central area of the specimen, show that the
278 mass elemental composition of MIBA is mostly comprised of oxygen (~23%), followed by
279 calcium (~15%), silicon (~9%), aluminium (~7%) and iron (~4%).

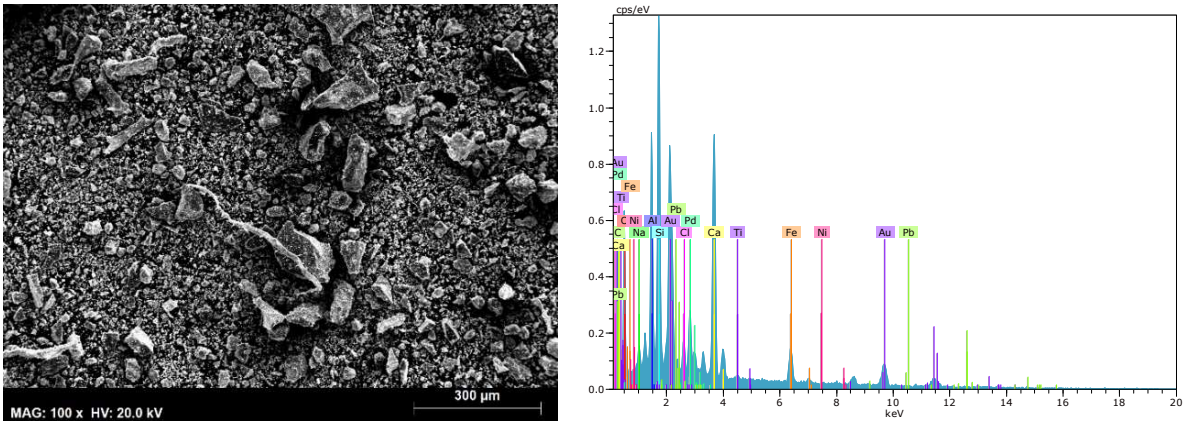

(a) (b)

280 Figure 3 - SEM (a) and EDS (b) of ground MIBA

281 The pozzolanicity of MIBA and FA was further characterized by the use of the modified
282 Chapelle test. It determined the content of unconsumed $Ca(OH)_2$, by titration with 0.1 M HCl
283 (reactions in equation 1 and 2), by the reactive phases present in FA and MIBA during 16 h of
284 reaction at 90 ± 5 °C of 2 g CaO grade laboratory and one gram of the precursor diluted in
285 distilled water.

$$CaO + 2HCl \rightarrow CaCl_2 + H_2O \quad (1)$$

$$Ca(OH)_2 + 2HCl \rightarrow CaCl_2 + 2H_2O \quad (2)$$

286 The following calculates the amount of mg $Ca(OH)_2$ / g of precursor (NBR-15895, 2010).

$$\frac{\text{mg } Ca(OH)_2}{\text{g precursor}} = \frac{28 \cdot (v_3 - v_2) \cdot F_c}{m_2} \times 1.32 \quad (3)$$

Where m_2 is the mass of the pozzolanic material (g), v_2 the volume of HCl consumed by the sample (ml); v_3 the volume of HCl consumed by the blank without MIBA as reference (ml); Fc the correction factor for a 0.1 M solution (ratio between the theoretical and experimental volumes of consumed HCl); and 1.32 the relation between the molecular masses of $Ca(OH)_2$ / CaO. The results showed values of 566 ± 59 mg and 445 ± 99 mg of $Ca(OH)_2$ / g of FA and MIBA, respectively. Although the average values are higher than the minimum limit of 436 mg $Ca(OH)_2$ / g of addition, established by Raverdy et al. (1980) for the classification of pozzolanic mineral additions, the standard deviation corresponding to MIBA suggests that some may be below the threshold. Future evaluation in this regard is warranted considering a much larger sample size (e.g. MIBA with changing age, various sizes and from different batches).

The amount of metallic Al was measured by means of its reaction with aqueous NaOH in an inverted test tube, which was connected through a glass tubing to a three-nozzle balloon. Equation 4 shows the chemical reaction behind this process and, in terms of the stoichiometric quantities (atomic and molecular weights), the quantities of each of the reactants and products generated in grams are presented in equation 5:

$$2Al + 2NaOH + 6H_2O \rightarrow 2NaAl(OH)_4 + 3\,H_2\uparrow \quad (4)$$

$$54\,g + 80\,g + 108\,g \rightarrow 236\,g + 6\,g\uparrow \quad (5)$$

Through the stoichiometry of the reaction, the measured volume of released H_2 allowed calculating the content in grams of metallic Al present in MIBA, after proper comparison with a control test using pure Al powder. 0.11 g of $H_2\uparrow$ are expected to be produced per each gram of Al consumed. 0.1 g of Al powder (control) or 10 g of MIBA were placed in an 800 ml solution of 2.5M NaOH and left to react for a period of 24 h. Three runs were performed; a displaced volume of 131.3 ± 5.0 ml was observed per 0.1 g of Al powder. The temperature at which the reaction was carried out corresponded to 43 °C (exothermic reaction of NaOH in water). The density of the H_2 at 43 °C and

1 atm. pressure is 0.0766 kg/m^3. From this property and the mass of H_2 produced by each gram of Al, it is was possible to determine the theoretical volume of H_2 generated:

$$v = \frac{m}{\rho}; \quad v_{H_2} = \frac{0{,}11\ g}{0{,}0000766\ g/ml} = 1436{,}03\ ml \tag{6}$$

The results for MIBA showed 63.3 ± 1.2 ml of released H_2, corresponding to 43.65 mg of metallic Al in 10 g of MIBA. Therefore, there are around 4.36 g of metallic Al for each kg of MIBA, which corresponds to 6.3 L of released $H_2\uparrow$ per kg of MIBA.

3.1.2 Aggregates

The particle size distributions and the results of apparent (ρ_a), rodded-dry (ρ_{rd}), saturated and surface-dried (ρ_{ssd}) and bulk (ρ_b) densities, and water absorption after 24 h (WA_{24}) for the two types of sand and RA are presented in Table 3. As expected, the density and water absorption of RA decreased and increased, respectively, in comparison with NA. Since the RA's particle size distribution was not equivalent to that of the combination of both fine and coarse sands, it was separated into different size fractions and subsequently combined in specific amounts. An additional test was carried out to ascertain the water absorption dynamics of these aggregates over time, following Rodrigues et al. (2013), using a hydrostatic scale. After 10 minutes, the RA presented a water absorption equivalent to 82% of that of its total capacity after 24 hours.

Table 3 - Physical properties of aggregates

Material		Fine sand	Coarse sand	Recycled aggregates
Density (kg/m^3)	ρ_a	2652	2636	2510
	ρ_{rd}	2624	2601	2040
	ρ_{ssd}	2634	2614	2230
	ρ_b	1544	1556	1217
WA_{24} (%)		0.40	0.51	9.33
Amount of material passing (%) in sieve (mm)	8.00	100	100	100
	4.00	100	96.6	100
	2.00	99.9	84.5	77.2
	1.00	98.9	42.6	42.3
	0.50	67.4	10.2	21.3
	0.250	9.5	3.3	8.3
	0.125	0.7	0.8	3.1
	0.063	0.3	0.3	1.8

3.2 Fresh state performance of mortars

3.2.1 Consistence

A consistence range of 170 ± 25 mm was adopted for all mixes to provide sufficient workability and stability. However, the reference mix using cement exhibited a spread of 223 mm. Nevertheless, these specimens are meant to provide an example of changing properties for equivalent mix design, but without direct comparison since the specimens were made using different methods and placed in changing curing conditions. For MIBA mixes with NA, the mixing methodology consisted of waiting 1 hour after the beginning of the procedure, so that a considerable portion of the reaction of metallic Al would take place, thereby avoiding the entrapment of most of the H_2 gas in the mix. Also, it should be noted that FA-containing mixes were produced with a liquid/binder ratio of 0.5, whereas that of MIBA-based mixes was equal to 0.65. Despite the efforts to maintain equivalent ratios with the use of a considerable amount of water-reducing admixtures of different types, alkali-activated MIBA mortars presented considerable water requirement and were unworkable at lower liquid/binder ratios. From this stage forward, even though FA- and MIBA-based mortars are presented in parallel, a direct comparison of results is not possible since they have different mix designs and thus varying porous microstructures. FA-NA mixes exhibited a slump flow of 185 mm, which decreased to 152 mm with the incorporation of RA. BA-NA and BA-RA mixes presented values of 173 mm and 164 mm, respectively. For both binders, the incorporation of RA induced, as expected, a less workable paste. Since the water absorption of RA was compensated by an additional amount of water, this decreased workability may likely have been due to the angularity of RA, relatively to NA, which resulted in a greater internal interparticle friction.

3.2.2 Fresh density

The control cement mortar presented a fresh-state density of 2248 g/dm^3. FA-NA and FA-RA mixes exhibited densities of 2260 g/dm^3 and 1970 g/dm^3, respectively, showing an expected

decrease with the incorporation of RA. These values were 1901 g/dm^3 and 1744 g/dm^3, for BA-NA and BA-RA, respectively. To understand the effect of the metallic Al reaction with the NaOH solution and the consequent H_2 entrapped in the mix (Figure 4), this test was made 1 h after the first test for BA-NA mixes; the fresh density increased to 2004 g/dm^3, corresponding to a 5% increase when compared to the lighter sample measured after 15 min of mixing, thus showing a considerable release of entrapped H_2 gas during that time.

Figure 4 - H_2 gas formation in the preparation of mortars

3.3 Hardened state performance of mortars

3.3.1 Compressive and flexural strength

The compressive strength of the control cement mortars after 7, 28 and 91 days were 43.9 MPa, 55.2 MPa and 66.2 MPa, respectively. Figure 5 presents the results of the compressive strength over time for alkali-activated FA specimens exposed to different curing regimens. The trend for FA mixes is in line with that observed by previous researchers (Atiş et al., 2015), in which higher initial strength was observed for mixes exposed to a longer thermal curing period. In this case, 70/48 mixes presented higher initial strength, followed by 90/24 and 70/24. This implies that, after a given temperature, the introduction of a higher amount of total energy (temperature × time)

(Elyamany et al., 2018) catalyses the nucleation of aluminosilicate particles with subsequent growth of zeolite-like structures (Duxson et al., 2007). However, over time, 70/24 and 90/24 FA-NA mixes showed greater strength development during the 91 days inferring continuous reactions of condensation-crystallization showing considerable interest from an energy-saving perspective.

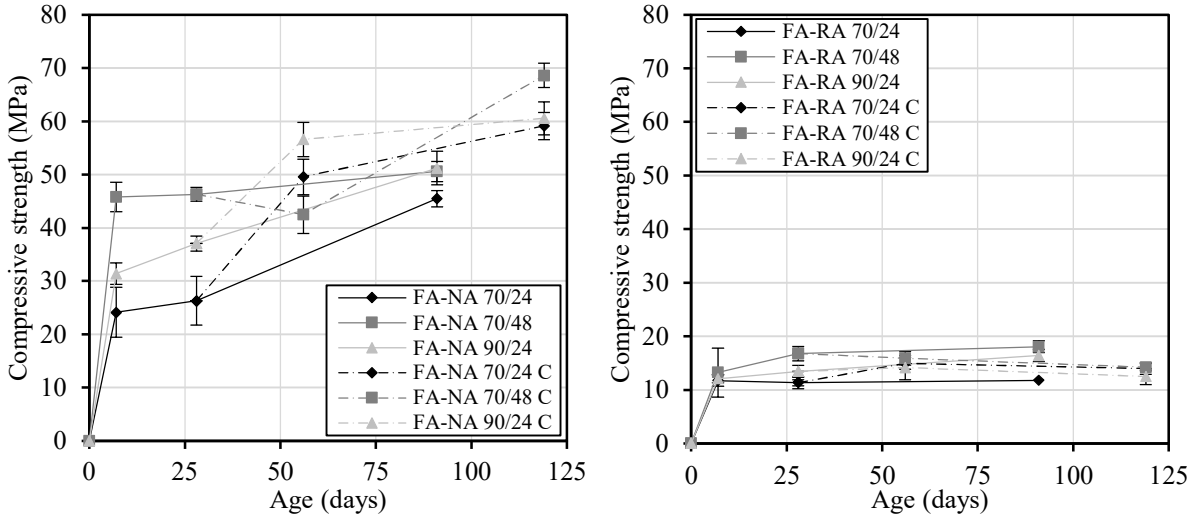

(a) (b)

Figure 5 - Compressive strength of alkali-activated FA containing (a) NA and (b) RA (C - carbonated)

Concerning FA-RA mixes (Figure 5b), the first trend was also observed, in which higher initial strength was presented by mixes exposed to a higher amount of energy, even though little strength development was observed after 28 days. A comparison of the compressive strength of FA-NA and FA-RA mixes shows that there was a loss of 57-64% after fully replacing the NA fraction. This level of strength loss was also observed in the study of Shi et al. (2012), wherein the incorporation of 100% coarse RA resulted in a mere strength loss of 10% in the cement-based concrete, whereas the same replacement level in FA-activated concrete led to a decrease of about 36%. Although some strength loss is expected with the incorporation of RA, the magnitude observed in this study and others (Shi et al., 2012) is greater than that typically observed in conventional cement-based mixes (Silva et al., 2014a). Besides the obvious higher porosity of RA relative to NA, this strength loss may have been due to partial adsorption of Na^+ and OH^- ions from the alkaline solution by the RA, thereby decreasing the total amount available to react with the binder. Consequently, these

ions may have catalysed an alkali-silica reaction of the RA, possibly leading to internal expansion and subsequent cracking. This aspect needs to be further analysed in future studies.

MIBA-containing mixes exposed to a 90/24 regime presented higher initial strength and constant development over time until 91 days, followed by the 70/48 and 70/24 mixes (Figure 6). When RA were incorporated, a similar plateau in strength development was observed; comparable compressive strength was seen after 7 and 91 days, regardless of the curing regime. Since a constant strength increase would be expected from the continuous condensation-crystallization of the precursor (observed for both FA-NA and BA-RA), additional analysis is needed to ascertain the impact of RA on strength development. Furthermore, it should be noted the oil-based release agent showed decreased efficacy when demoulding alkali-activated mortars (mostly those exposed to a 90/24 curing), which resulted in the detachment of part of the material. Additional analysis should be carried out to ascertain the compatibility of release agents for alkali-activated materials.

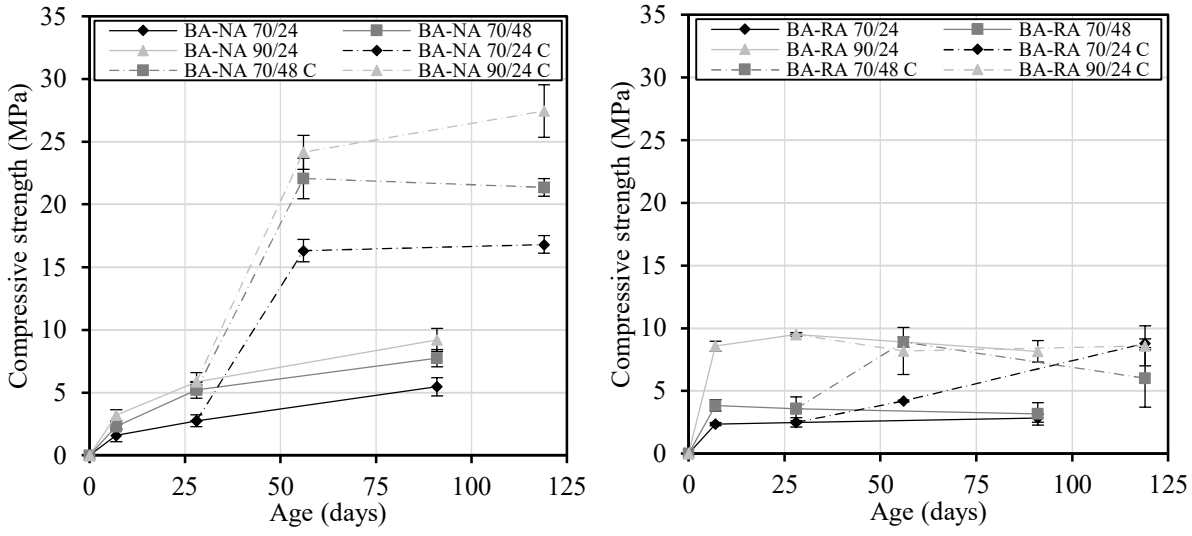

(a) (b)

Figure 6 - Compressive strength of alkali-activated MIBA containing (a) NA and (b) RA (C - carbonated)

Even though a direct comparison is not possible between FA and MIBA mixes since they were made with different mix designs, the strength development of the latter was markedly lower considering the increase in liquid/binder ratio. The decreased strength is due to the aforementioned

400 reaction of metallic Al with NaOH, leading to considerable entrapped H_2 gas, which naturally
401 affected the macrostructural performance of the specimens. Furthermore, the Chapelle test sug-
402 gests that MIBA contains a smaller portion of amorphous silica and alumina when compared to
403 FA, which naturally means that it is a less reactive material.

404 A resistance to carbonation test was initially envisaged at the beginning of this experimental cam-
405 paign to understand the velocity of pH level decrease as the specimens were exposed to CO_2 gas.
406 However, the test results were inconclusive since all specimens were carbonated after just 28 days
407 (i.e. none of the alkali activated materials presented a pinkish hue), whereas the control cement
408 mortars presented depths 3.7 mm and 4.4 mm after 28 and 91 days, respectively. A faster pH de-
409 crease due to carbonation was expected since AAM do not usually have $Ca(OH)_2$ available to car-
410 bonate (Palacios and Puertas, 2006) and the amount of OH^- ions, from the NaOH solution, de-
411 creases over time as they react with Si and Al species in the destruction-coagulation process (Provis
412 and van Deventer, 2014). Nevertheless, all specimens intended for carbonation testing were sub-
413 jected to flexural and compressive strength testing to ascertain the effect of carbonation on the
414 mechanical performance of these mortars. Figure 5 and Figure 6 also present the strength develop-
415 ment over time of the same mixes. Until the age of 28 days, all specimens were subjected to the
416 same curing environment and then exposed to a CO_2-rich environment for 28 days and 91 days
417 (total age of 56 days and 112 days, respectively). Within those 28 and 91 days in the carbonation
418 chamber, a clear strength increase was observed. When compared with the specimens exposed to
419 28 days of normal curing in an environmental chamber, strength increased about 20 MPa for FA-
420 NA 70/24 and 90/24. For unknown reasons, this was not observed for FA-NA 70/48, which pre-
421 sented strength reduction after 28 days, even though it showed nearly 70 MPa after 91 days (control
422 cement mortar presented a 91-day compressive strength of 69.2 MPa). All 112-day carbonated
423 mixes showed strength gain between 18% and 36% when compared with 91-day uncarbonated
424 ones. A more prominent strength gain was observed in BA-NA mixes (Figure 6a), with increases

of 275% to 306% (equivalent to absolute variations between 11 MPa and 18 MPa), wherein the BA-NA 90/24 presented a compressive strength of about 28 MPa after 91 days of carbonation. This considerable strength gain in both FA-NA and BA-NA mixes first starts with the dissolution of CO_2 into carbonic acid (H_2CO_3), decreasing pH level locally, which subsequently led to decomposition of e.g. alkaline metal-based compounds, $Ca(OH)_2$, silicates and aluminates in the matrix. In the case of Ca-bearing compounds (mostly for MIBA-based mortars), a decalcification followed by precipitation of calcium carbonate polymorphs ($CaCO_3$ in the form of vaterite, aragonite or calcite) and polymerization process of amorphous SiO_2 (see equation 1 and 2, where CH - $Ca(OH)_2$, C - CaO, $\overline{C}$ - CO_2, S - SiO_2, H - H_2O) (Morandeau et al., 2014).

$$\mathrm{CH} + \overline{\mathrm{C}} \rightarrow \mathrm{C}\overline{\mathrm{C}} + \mathrm{H} \quad (1)$$

$$\mathrm{C}_x S_y \mathrm{H}_z + x\overline{\mathrm{C}} \rightarrow x\mathrm{C}\overline{\mathrm{C}} + y\mathrm{SH}t + (z - yt)\mathrm{H} \quad (2)$$

Ca^{2+} ions, from the decalcification process, tend to migrate and precipitate in the form of $CaCO_3$ in adjacent interstitial spaces thereby increasing the density of the matrix, which ultimately results in enhanced mechanical performance. Additionally, the SiO_2 gel is also likely to have a predominant role in the overall strength increase of the microstructure, since the Si-O bonds of the Q^3 and Q^4 SiO_4 tetrahedra have a considerable bond strength (Li et al., 2018). Even though AAM based on class F FA are likely to present low content of Ca-bearing phases due to the low CaO content of the precursor (i.e. ~4.5%), they contain C-(N-)A-S-H, which may decalcify and lead to the formation of $CaCO_3$ and silica gel. The N-A-S-H gel is considered to be stable with ensuing diffusion of CO_2 in the microstructure. Therefore, it is likely that the strength increase of FA-based specimens occurred due to formation of carbonation products from the reaction of Na^+ and Ca^{2+} ions in the pore aqueous solution into sodium bicarbonate (Nahcolite - $NaHCO_3$) and gaylusite ($Na_2Ca(CO_3)_2{\cdot}_5H_2O$). Since this led to the depletion of cations available to preserve the equilibrium of the metastable N-A-S-H gel, neighbouring groups Si-OH, Si-ONa, Al-OH or Al-ONa condense and merge to Si-O-Si or Si-O-Al gels thereby increasing the degree of

polymerization (Nedeljković et al., 2018). Indeed, looking at the results of the XRD analysis of carbonated and uncarbonated pastes equivalent to BA-NA 70/24 mixes (Figure 7), the XRD spectrum of the uncarbonated mix demonstrated the occurrence of polymerization reactions corroborated by the presence of hydrated sodium aluminosilicate ($Na_6[AlSiO_4]_6 \cdot 4H_2O$). Hydrated sodium carbonate ($Na_2CO_3 \cdot 7H_2O$) was also identified, as well as crystalline SiO_2, which came from the unreacted precursor and is present in all samples. The carbonated paste contained calcium silicate hydrate ($Ca_{1.5}SiO_{3.5}\,xH_2O$) or C-S-H, aragonite ($CaCO_3$) and nahcolite ($NaHCO_3$).

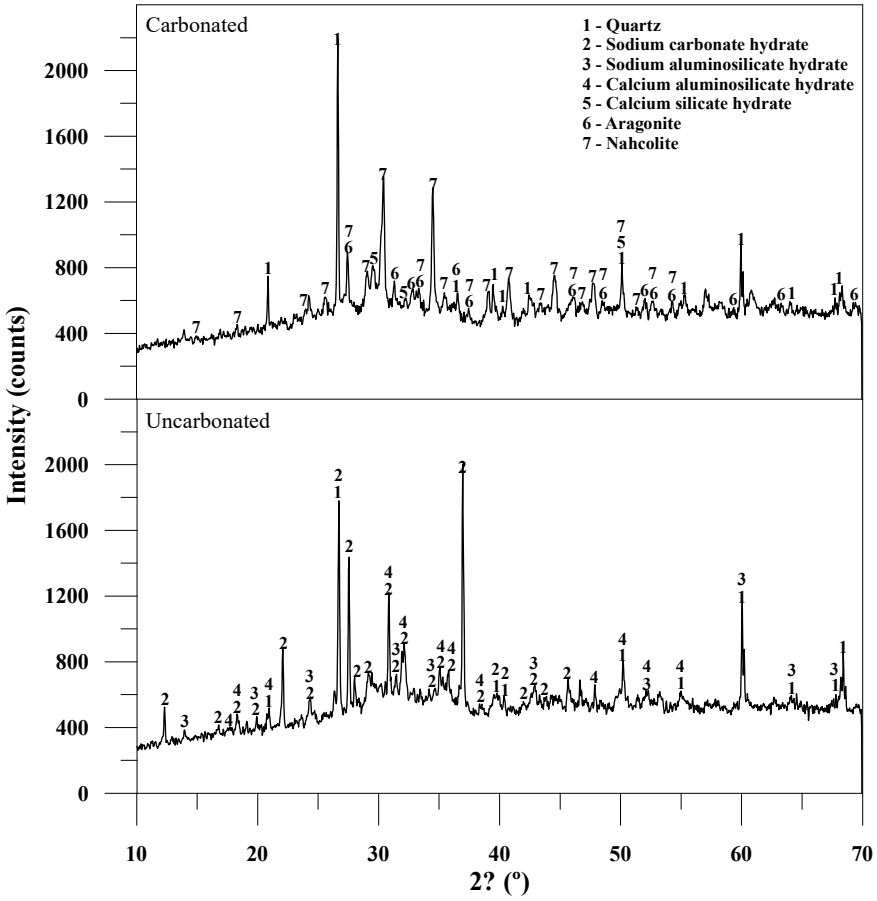

Figure 7 - XRD spectrum of carbonated and uncarbonated BA-NA 70/24

Concerning FA-RA and BA-RA mixes, although a strength gain was also expected with ensuing carbonation since RA have higher content of Ca-bearing phases than NA, equivalent or slightly enhanced performance was observed. This can be explained by the likely inexistence of $Ca(OH)_2$ in the RA's adhered mortar, which would have been almost entirely carbonated before its use

(Gonçalves et al., 2020). Also, in another experimental campaign, carried out in parallel to this one, almost all carbonated specimens exhibited strength loss from 28 to 91 days, despite an initial increase in the first 28 days. The carbonation process may have generated tensions around unreacted particles in carbonated areas due to carbonation-induced shrinkage. This phenomenon, in combination with increased shrinkage of mixes with RA, may have caused extensive micro-cracking thereby leading to strength loss after long exposure to a CO_2-rich environment (Bernal et al., 2013).

Regarding the results of the flexural strength test, the control cement mortars presented values of 5.3 MPa, 6.9 MPa and 6.8 MPa after 7, 28 and 91 days, respectively. AAM based on FA demonstrate slow strength development during the first 28 days, due to the slow polymerization reactions over time (Olivia and Nikraz, 2012). However, enhanced flexural strength can be seen after 28 days and 91 days (Figure 8), because of the physical strength of the three-dimensional structure as a result of the polymerization reactions.

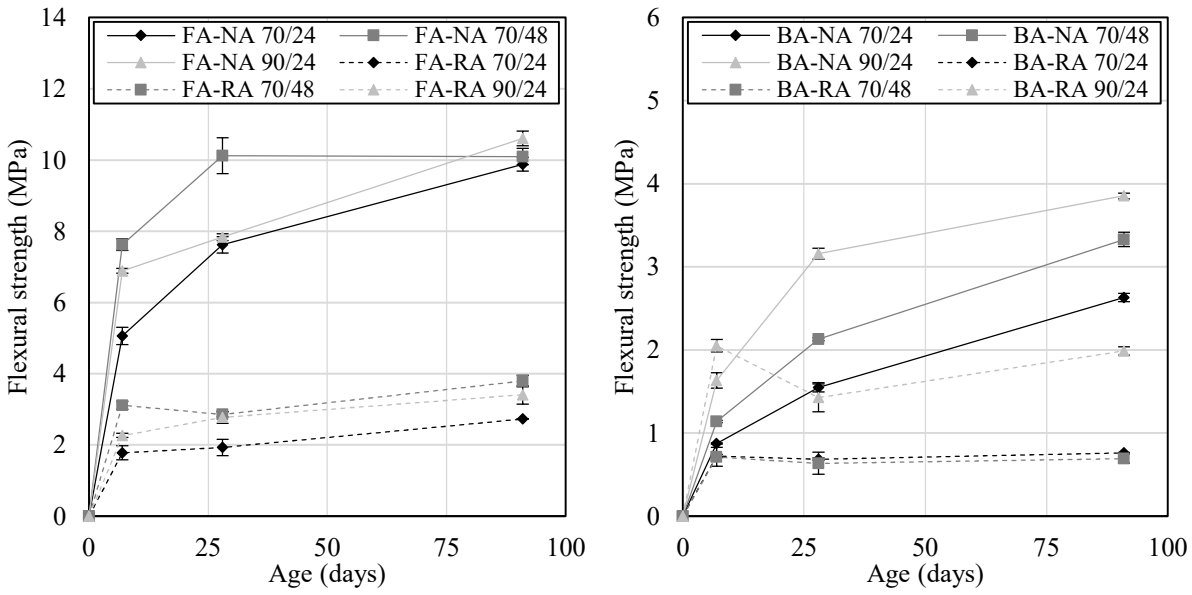

(a) (b)

Figure 8 - Flexural strength of (a) FA and (b) MIBA mixes

Alkali activated FA mixes showed considerably higher values. The results of the flexural strength test showed a similar trend to that of the compressive strength; in FA-NA mixes, higher strength

476 was achieved by those cured in 70/48 conditions, followed, by 90/24 and 70/24, the difference
477 between which was offset until 91 days. This suggests that, even though the 70/48 curing condi-
478 tion could be deemed the optimum regime to provide higher initial strength, in the light of the
479 equivalent performance after 91 days, 70/24 could be considered more environmental-friendly
480 for a given target behaviour. The incorporation of RA led to considerable strength decrease (i.e.
481 loss of about 65% between FA-RA and FA-NA mixes). Again, even though this trend was ex-
482 pected, the incorporation of RA does not usually lead to such losses (Silva et al., 2015). Alkali
483 activated MIBA mixes showed decreased performance due to the corrosion reactions of metallic
484 Al and the lower amount of reactive phase. Nevertheless, a steady increase in flexural strength
485 can be seen even after 91 days, similar to those of the compressive strength.

486 ### 3.3.2 Modulus of elasticity

487 The control cement mixes presented dynamic moduli of elasticity of 35.6 GPa, 38.4 GPa and 40.7
488 GPa after 7, 28 and 91 days, respectively. Figure 9 presents the results of the dynamic modulus of
489 elasticity test for alkali-activated FA and MIBA mixes.

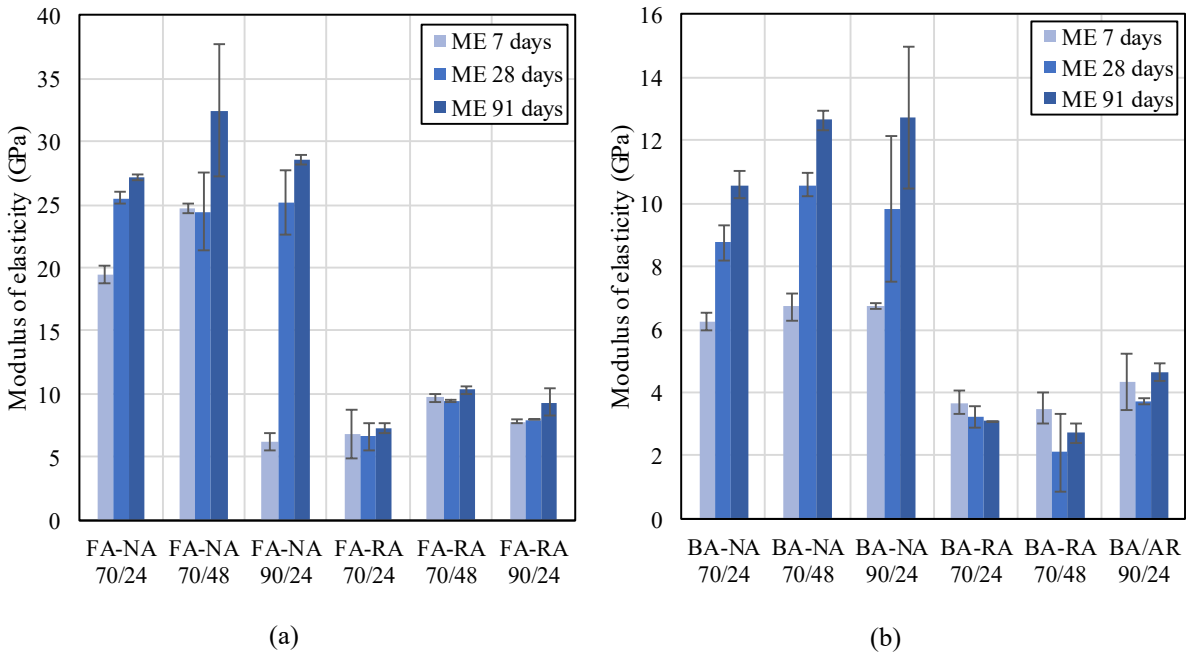

490 Figure 9 - Dynamic modulus of elasticity of (a) FA and (b) MIBA mixes

Regardless of the curing condition, FA-NA mixes showed about 35% lower moduli of elasticity when compared to the 28-day value of the control cement mix. As expected, FA and MIBA specimens subjected to a 70/48 curing presented higher moduli of elasticity in comparison with those from 90/24 and 70/24 regimens. An immediately perceivable difference can be seen between mixes with and without RA; its incorporation led to a decrease of around 70%. Although a notable decrease would be expected as RA demonstrate greater deformability in comparison with NA, the magnitude is higher than that typically observed for conventional cement-based mixes (Silva et al., 2016). Also, whilst FA-NA and BA-NA mixes presented a continuous increase over time, those with RA plateaued after 7 days.

3.3.3 Ultrasonic pulse velocity

Table 4 shows the results of the ultrasonic pulse velocity test. For two of the specimens (i.e. 7-day FA-NA 70/24 and 28-day BA-NA 70/48), the test was not possible due to irregular surfaces and loss of material, making them unrepresentative. None of the 91-day values was measured due to technical difficulties of the equipment. The results can be well correlated with those of the dynamic moduli of elasticity. Again, 70/48 curing provided initially increased densification leading to higher moduli of elasticity with progressively lower difference until 91 days. As expected, all samples made with RA had lower results when compared with the control NA mixes. The results of the control cement mortars were 4126 m/s, 4586 m/s and 4565 m/s after 7, 28 and 91 days, respectively.

Table 4 - Ultrasonic pulse velocity of FA and MIBA mixes

Mix		Ultrasonic pulse velocity (m/s)		
		7 days	28 days	91 days
FA-NA	70/24	-	3613	3584
	70/48	3597	3743	3813
	90/24	2939	2632	3756
FA-RA	70/24	2341	1755	2439
	70/48	2521	2181	2561
	90/24	2132	2127	1972
BA-NA	70/24	1982	2183	-
	70/48	2830	-	-
	90/24	2068	2379	-
BA-RA	70/24	1623	1590	-
	70/48	1543	1860	-
	90/24	2362	2147	-

3.3.4 Shrinkage

Figure 10 presents the dimensional variation over time of the alkali-activated mixes. An initial analysis of the results of the FA and MIBA mixes shows that there was a greater dispersion of the latter with changing curing conditions and incorporation of RA. FA-NA 70/24 was considered as the most stable material with the least variation over time (~200 µm/m after 91 days). FA-NA 70/48 and 90/24 showed equivalent performance and a final shrinkage strain (i.e. 500-600 µm/m) equivalent to that expected from typical cement mortars (Gonçalves et al., 2019). As expected, due to the greater deformability of RA (Silva et al., 2014b), the incorporation of RA led to higher shrinkage strain. However, it should be noted that unusual isolated expansion phenomena occurred in these specimens at certain ages (Figure 10a), which may indicate changing conditions of the curing environment. This may have resulted in lower than expected final shrinkage strains.

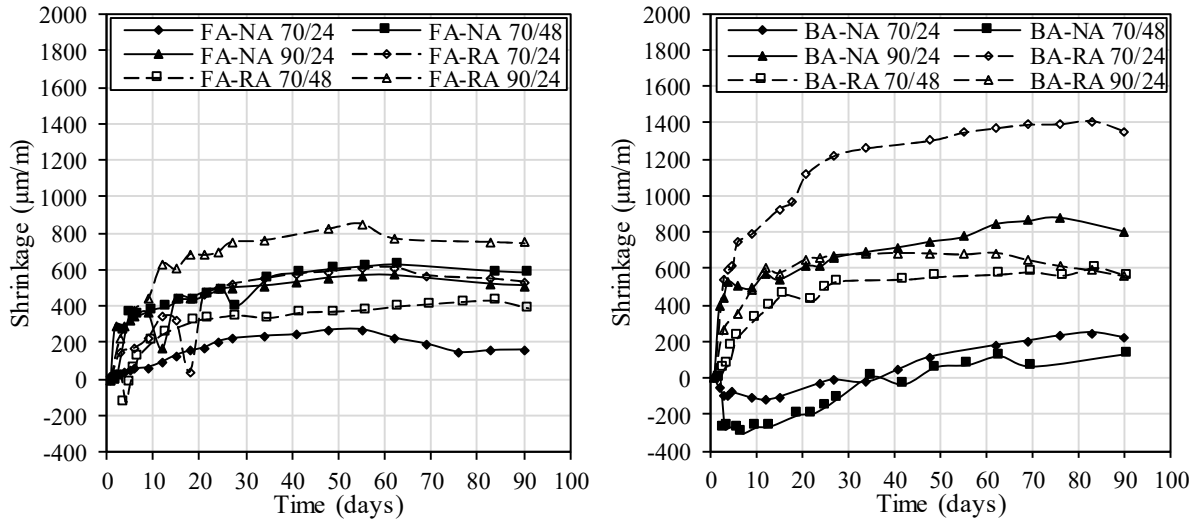

(a) (b)

Figure 10 - Dimensional stability of alkali-activated (a) FA and (b) MIBA mixes

Although BA mixes were expected to present greater shrinkage due to the lower content of amorphous phases and formation of H_2 gas, most of them showed the equivalent performance of FA mixes. The BA-RA 70/24 mix presented notably higher shrinkage strain (~1400 µm/m) when compared with that of the BA-RA 70/48 and 90/24 mixes (~600 µm/m). However, this

discrepancy was observed in BA-NA 90/24, which presented a final shrinkage strain of about 800 μm/m. Additionally, BA-NA 70/24 and 70/48 showed considerable expansion in the first 3-5 days of curing and started to shrink after that. The expansion may have been due to the formation of H_2 gas from the reaction of metallic Al, which did not corrode entirely in the thermal curing process due to the lower temperature input. However, since this trend was not observed in BA-RA mixes, additional testing is required to comprehend the effect of both MIBA activation and RA incorporation on this property.

3.3.5 Water absorption by capillary action

Figure 11 presents the water absorption by means of capillary action of FA mixes. Although this test was also carried out on BA mixes, because of a change in the water's colour (brownish hue) and considerable efflorescence and mass loss of the specimens, the results would not be representative of the property and were thus discarded. Although FA-NA 70/24 presented the lowest sorptivity over time, little difference was observed for mixes exposed to different curing regimen. As expected from mixes containing RA and similar to the results of Nuaklong et al. (2016), the incorporation of RA led to greater internal porosity and pore interconnectivity, thereby leading to higher water absorption by capillary action. A more expected trend was observed specimens containing RA regarding the effect of the thermal curing regime; FA-RA 70/48 and 70/24 presented the lowest and highest values respectively, which can be well correlated with the results of the compressive and flexural strength tests as well as those of the dynamic moduli of elasticity. The control cement mortar showed a mass gain per unit area of about 12×10^{-3} g/mm^2 after 72 hours, being almost twice more than that of FA-NA mixes with equivalent mix design. This infers that the alkali activation of FA is capable of producing a more tortuous and less interconnected porous network (Shi et al., 2012).

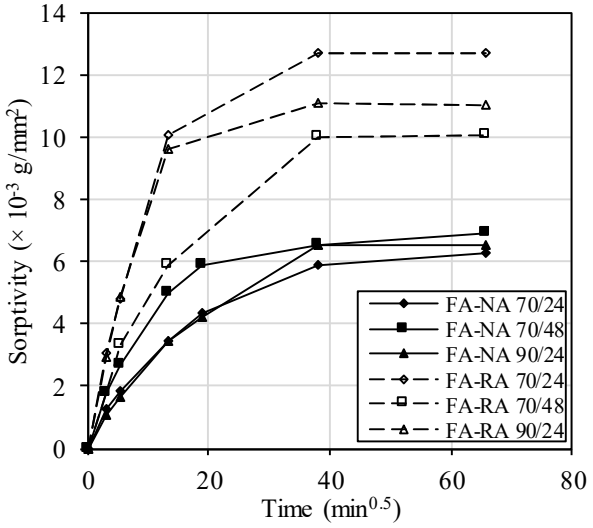

Figure 11 - Water absorption by capillary action of FA mixes

Concerning the poor physical stability of the MIBA-based mortars when exposed to the test, leaching of constituents was observed, which led to a brownish colour of the test water, probably due to leached ferrous compounds. Because of the environmental impacts of this phenomenon, an upcoming experimental campaign on the leaching behaviour of alkali-activated MIBA-based mortars is expected to be carried out in the near future within the scope of the research project PTDC/ECI-CON/29196/2017 (RInoPolyCrete). Ferrous compounds, apart from not dissolving in an alkaline environment, can form bonds with Al in a spinel system or with iron-rich glasses, decreasing the available amount of Al and Si for the polymerization reactions thereby leading to decreased strength (Chen-Tan et al., 2009) and the possibly greater likelihood of being leached. The precipitated material, resulting from the evaporation of water from each test, was analysed by XRD to understand the nature of the leached compounds from BA-NA specimens (Figure 12). It mostly contained sodium carbonates (in the form of thermonatrite - $Na_2CO_3 \cdot H_2O$ - ICDD # 001-1015 and trona -$Na_3H(CO_3)_2 \cdot 2H_2O$ - ICDD # 029-1447) and halite (NaCl - ICDD # 001-0994). These results suggest a considerable amount of Na^+ ions in the solution, which did not partake in the reaction with the precursor (Criado et al., 2005; Provis and van Deventer, 2014), leached into the test water and reacted directly with atmospheric CO_2.

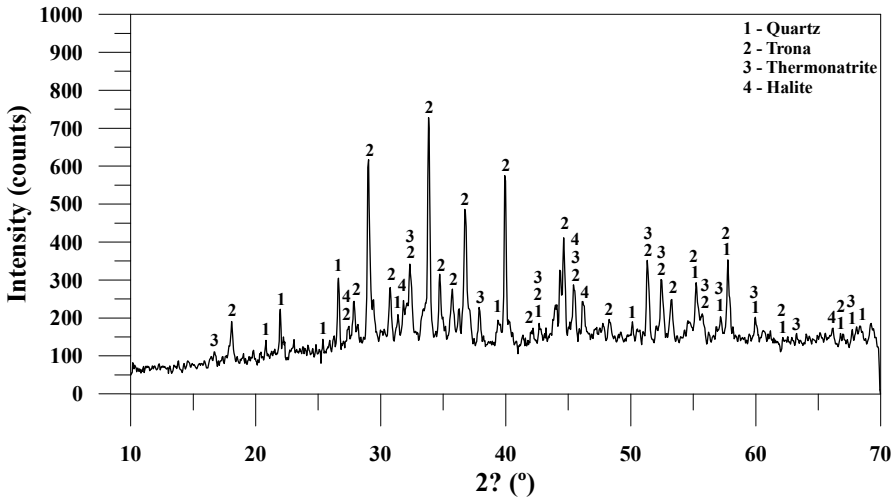

Figure 12 - XRD analysis of efflorescence precipitates from BA-NA specimens

4 Conclusions

The effect of RA on the mechanical and durability-related performance of alkali-activated FA and MIBA mixes was evaluated. MIBA has a similar chemical composition to that expected from class C FA. However, it is comprised of a lower quantity of amorphous material (primarily from waste glass), thereby presenting poorer reactivity in an alkaline medium when compared to FA. Additionally, MIBA contains a considerable amount of ferrous metals that could be further extracted at the treatment facility. Still, since the electromagnetic separation of non-ferrous metals through Eddy current is not very effective, metallic Al is always likely to be present in MIBA. As a result, it will react with the OH^- ions from the NaOH solution causing the formation of H_2 gas, which becomes entrapped in the fresh mix. Furthermore, after the thermal curing process, which catalyses this reaction and promotes setting, excessive expansion and internal porosity is likely to be observed. This higher porosity, in combination with the lower reactivity of MIBA, leads to a considerable decline in performance. However, notable performance enhancement can be observed in specimens exposed to accelerated carbonation. This occurs as a result of the decalcification of Ca-bearing phases and consequent precipitation of $CaCO_3$ polymorphs, as well as from the carbonation of Na^+ in the pore solution into sodium carbonates, both of which increase the degree of polymerization of Si-O-Si and Si-O-Al gels, thereby significantly increasing

the material's strength. The incorporation of RA, as expected, led to an overall decline in performance, but its magnitude was greater than that typically observed by conventional cement-based concrete and mortar. This infers the presence of an underlying nefarious phenomenon, possibly the extensive micro-cracking due to alkali-silica reaction of RA with the alkaline activator, which requires further evaluation in upcoming experimental campaigns.

Acknowledgements

The authors gratefully acknowledge the support of the CERIS Research Institute, IST - University of Lisbon and FCT - Foundation for Science and Technology, through the research project PTDC/ECI-CON/29196/2017 "Recycled Inorganic Polymer Concrete: Towards a fully recycled and cement-free concrete" (RInoPolyCrete) and CERENA Strategic Project UID/ECI/04028/2013. The authors would also like to acknowledge the support of Valorsul, EDP, SIKA and Secil for part of the materials provided for this experimental campaign.

Data availability

The raw/processed data required to reproduce these findings cannot be shared at this time as they are part of an ongoing study.

References

Alonso, M.M., Rodríguez, A., Puertas, F., 2018. Viability of the use of construction and demolition waste aggregates in alkali-activated mortars. Materiales de Construcción 68(331), e164.

ASTM-C618, 2019. Standard specification for coal fly ash and raw or calcined natural pozzolan for use in concrete. American Society for Testing and Materials, West Conshohocken, Pennsylvania, USA, 5 p.

ASTM-E1876, 2015. Standard test method for dynamic Young's modulus, shear modulus, and Poisson's ratio by impulse excitation of vibration. American Society for Testing and Materials, USA, 17 p.

Atiş, C.D., Görür, E.B., Karahan, O., Bilim, C., İlkentapar, S., Luga, E., 2015. Very high strength (120MPa) class F fly ash geopolymer mortar activated at different NaOH amount, heat curing temperature and heat curing duration. Constr. Build. Mater. 96, 673-678.

Bernal, S.A., Provis, J.L., Walkley, B., San Nicolas, R., Gehman, J.D., Brice, D.G., Kilcullen, A.R., Duxson, P., van Deventer, J.S.J., 2013. Gel nanostructure in alkali-activated binders based on slag and fly ash, and effects of accelerated carbonation. Cem. Concr. Res. 53, 127-144.

CEU, 1998. Council Directive 98/83/EC of 3 November 1998 on the quality of water intended for human consumption. Official Journal of the European Communities 330, 32-54.
Chen-Tan, N.W., Van Riessen, A., LY, C.V., Southam, D.C., 2009. Determining the reactivity of a fly ash for production of geopolymer. J. Am. Ceram. Soc. 92(4), 881-887.
Chen, Z., Liu, Y., Zhu, W., Yang, E.-H., 2016. Incinerator bottom ash (IBA) aerated geopolymer. Construction and Building Materials 112, 1025-1031.
Criado, M., Palomo, A., Fernández-Jiménez, A., 2005. Alkali activation of fly ashes. Part 1: Effect of curing conditions on the carbonation of the reaction products. Fuel 84(16), 2048-2054.
Cristelo, N., Segadaes, L., Coelho, J., Chaves, B., Sousa, N.R., Lopes, M.D., 2020. Recycling municipal solid waste incineration slag and fly ash as precursors in low-range alkaline cements. Waste Manage. 104, 60-73.
Davidovits, J., 1994. Properties of geopolymer cements, Proceedings First International Conference on Alkaline Cements and Concretes, Scientific Research Institute on Binders and Materials, Kiev State Technical University, Kiev, Ukraine, 131-149 p.
Dhir, R.K., De Brito, J., Lynn, C.J., Silva, R.V., 2018. Sustainable construction materials: Municipal incinerator bottom ash. Woodhead Publishing, Duxford, UK.
Duxson, P., Fernández-Jiménez, A., Provis, J.L., Lukey, G.C., Palomo, A., van Deventer, J.S.J., 2007. Geopolymer technology: the current state of the art. Journal of Materials Science 42(9), 2917-2933.
Elyamany, H.E., Abd Elmoaty, A.E.M., Elshaboury, A.M., 2018. Setting time and 7-day strength of geopolymer mortar with various binders. Constr. Build. Mater. 187, 974-983.
EN-196-1, 2005. Methods of testing cement - Part 1: Determination of strength. Comité Européen de Normalisation (CEN), Brussels, Belgium, 36 p.
EN-450-1, 2012. Fly ash for concrete. Definition, specifications and conformity criteria. Comité Européen de Normalisation (CEN), Brussels, Belgium, 34 p.
EN-1015-1, 1999. Methods of test for mortar for masonry - Part 1: Determination of particle size distribution (by sieve analysis). Comité Européen de Normalisation (CEN), Brussels, Belgium, 8 p.
EN-1015-2, 1999. Methods of test for mortar for masonry - Part 2: Bulk sampling of mortars and preparation of test mortars. Comité Européen de Normalisation (CEN), Brussels, Belgium, 8 p.
EN-1015-3, 1999. Methods of test for mortar for masonry - Part 3: Determination of consistence of fresh mortar (by flow table). Comité Européen de Normalisation (CEN), Brussels, Belgium, 10 p.
EN-1015-6, 1999. Methods of test for mortar for masonry - Part 6: Determination of bulk density of fresh mortar. Comité Européen de Normalisation (CEN), Brussels, Belgium, 8 p.
EN-1015-11, 1999. Methods of test for mortar for masonry - Part 11: Determination of flexural and compressive strength of hardened mortar. Comité Européen de Normalisation (CEN), Brussels, Belgium, 12 p.
EN-1015-13, 1993. Methods of test for mortar for masonry - Part 13: Determination of dimensional stability of hardened mortars. Comité Européen de Normalisation (CEN), Brussels, Belgium, 20 p.
EN-1015-18, 2002. Methods of test for mortar for masonry - Part 18: Determination of water absorption coefficient due to capillary action of hardened mortar. Comité Européen de Normalisation (CEN), Brussels, Belgium, 12 p.
EN-1097-3, 1998. Tests for mechanical and physical properties of aggregates - Part 3: Determination of loose bulk density and voids. Comité Européen de Normalisation (CEN), Brussels, Belgium, 10 p.

668 EN-1097-5, 2008. Tests for mechanical and physical properties of aggregates - Part 5:
669 Determination of the water content by drying in a ventilated oven. Comité Européen de
670 Normalisation (CEN), Brussels, Belgium, 54 p.
671 EN-12504-4, 2004. Testing concrete. Determination of ultrasonic pulse velocity. Comité
672 Européen de Normalisation (CEN), Brussels, Belgium, 18 p.
673 Fang, G., Ho, W.K., Tu, W., Zhang, M., 2018. Workability and mechanical properties of alkali-
674 activated fly ash-slag concrete cured at ambient temperature. Constr. Build. Mater. 172, 476-
675 487.
676 Ferraro, A., Farina, I., Race, M., Colangelo, F., Cioffi, R., Fabbricino, M., 2019. Pre-treatments
677 of MSWI fly-ashes: a comprehensive review to determine optimal conditions for their reuse
678 and/or environmentally sustainable disposal. Reviews in Environmental Science and
679 Bio/Technology 18(3), 453-471.
680 Ferraz, E., Andrejkovičová, S., Hajjaji, W., Velosa, A.L., Silva, A.S., Rocha, F., 2015.
681 Pozzolanic activity of metakaolins by the French Standard of the modified Chapelle Test: A
682 direct methodology. Acta Geodynamicaet Geometerialia Aspects(12), 289-298.
683 Galiano, Y.L., Pereira, C.F., Vale, J., 2011. Stabilization/solidification of a municipal solid
684 waste incineration residue using fly ash-based geopolymers. J. Hazard. Mater. 185(1), 373-
685 381.
686 Gonçalves, T., Silva, R.V., de Brito, J., Fernández, J.M., Esquinas, A.R., 2019. Hydration of
687 reactive MgO as partial cement replacement and its influence on the macroperformance of
688 cementitious mortars. Advances in Materials Science and Engineering Article ID 9271507, 12.
689 Gonçalves, T., Silva, R.V., de Brito, J., Fernández, J.M., Esquinas, A.R., 2020. Mechanical
690 and durability performance of mortars with fine recycled concrete aggregates and reactive
691 magnesium oxide as partial cement replacement. Cem. Concr. Compos. 105, 103420.
692 Huang, G., Ji, Y., Zhang, L., Li, J., Hou, Z., 2018. The influence of curing methods on the
693 strength of MSWI bottom ash-based alkali-activated mortars: The role of leaching of OH^- and
694 free alkali. Constr. Build. Mater. 186, 978-985.
695 Huang, G., Yang, K., Sun, Y., Lu, Z., Zhang, X., Zuo, L., Feng, Y., Qian, R., Qi, Y., Ji, Y., Xu,
696 Z., 2020. Influence of NaOH content on the alkali conversion mechanism in MSWI bottom ash
697 alkali-activated mortars. Constr. Build. Mater. 248.
698 Kurda, R., Silva, R.V., de Brito, J., 2020. Incorporation of alkali-activated municipal solid
699 waste incinerator bottom ash in mortar and concrete: A critical review. Materials 13(15), 1-24.
700 Li, Z., He, Z., Shao, Y., 2018. Early age carbonation heat and products of tricalcium silicate
701 paste subject to carbon dioxide curing. Materials 11(5), 730.
702 LNEC-E391, 1993. Concrete: determination of carbonation resistance (in Portuguese).
703 National Laboratory in Civil Engineering (LNEC - Laboratório Nacional de Engenharia Civil)
704 Lisbon, Portugal, 2 p.
705 Lynn, C.J., Dhir, R.K., Ghataora, G.S., 2017. Municipal incinerated bottom ash use as a cement
706 component in concrete. Mag. Concrete Res. 69(10), 512-525.
707 Morandeau, A., Thiéry, M., Dangla, P., 2014. Investigation of the carbonation mechanism of
708 CH and C-S-H in terms of kinetics, microstructure changes and moisture properties. Cem.
709 Concr. Res. 56, 153-170.
710 NBR-15895, 2010. Materiais pozolânicos - Determinação do teor de hidróxido de cálcio fixado
711 - Método de Chapelle modificado. Brazilian Association for Technical Norms (Associação
712 Brasileira de Normas Técnicas - ABNT), Rio de Janeiro, Brasil, 10 p.
713 Nedeljković, M., Zuo, Y., Arbi, K., Ye, G., 2018. Carbonation resistance of alkali-activated
714 slag under natural and accelerated conditions. Journal of Sustainable Metallurgy 4(1), 33-49.
715 Nørgaard, K.P., Hyks, J., Mulvad, J.K., Frederiksen, J.O., Hjelmar, O., 2019. Optimizing large-
716 scale ageing of municipal solid waste incinerator bottom ash prior to the advanced metal

recovery: Phase I: Monitoring of temperature, moisture content, and CO2 level. Waste Manage. 85, 95-105.
Nuaklong, P., Sata, V., Chindaprasirt, P., 2016. Influence of recycled aggregate on fly ash geopolymer concrete properties. J. Clean. Prod. 112, Part 4, 2300-2307.
Olivia, M., Nikraz, H., 2012. Properties of fly ash geopolymer concrete designed by Taguchi method. Mater. Des. 36, 191-198.
Palacios, M., Puertas, F., 2006. Effect of carbonation on alkali-activated slag paste. J. Am. Ceram. Soc. 89(10), 3211-3221.
Provis, J.L., 2018. Alkali-activated materials. Cem. Concr. Res. 114, 40-48.
Provis, J.L., van Deventer, J.S.J., 2014. Alkali Activated Materials - State-of-the-Art Report, RILEM TC 224-AAM. Springer, Dordrecht, The Netherlands.
Raverdy, M., Brivot, F., Paillere, A.M., Dron, R., 1980. Appreciation of pozzolanic reactivity of secondary components (in French), 7eme Congres International de la Chimie Des Ciments Paris Francep.
Rodrigues, F., Evangelista, L., de Brito, J., 2013. A new method to determine the density and water absorption of fine recycled aggregates. Materials Research 16, 1045-1051.
Rowlatt, J., 2019. Coal: Is this the beginning of the end? (accessed 30/06/2020).
Shi, X.S., Collins, E.G., Zhao, X.L., Wang, Q.Y., 2012. Mechanical properties and microstructure analysis of fly ash geopolymeric recycled concrete. J. Hazard. Mater. 237, 20-29.
Silva, R.V., de Brito, J., Dhir, R.K., 2014a. The influence of the use of recycled aggregates on the compressive strength of concrete: a review. European Journal of Environmental and Civil Engineering 19(7), 825-849.
Silva, R.V., de Brito, J., Dhir, R.K., 2014b. Properties and composition of recycled aggregates from construction and demolition waste suitable for concrete production. Constr. Build. Mater. 65, 201-217.
Silva, R.V., de Brito, J., Dhir, R.K., 2015. Tensile strength behaviour of recycled aggregate concrete. Constr. Build. Mater. 83, 108-118.
Silva, R.V., de Brito, J., Dhir, R.K., 2016. Establishing a relationship between modulus of elasticity and compressive strength of recycled aggregate concrete. J. Clean. Prod. 112, 2171-2186.
Silva, R.V., de Brito, J., Lynn, C.J., Dhir, R.K., 2017. Use of municipal solid waste incineration bottom ashes in alkali-activated materials, ceramics and granular applications: A review. Waste Manage. 68, 207-220.
Singh, R., 2012. Chapter 5 - Production of steel Applied Welding Engineering: Processes, Codes, and Standards. Butterworth-Heinemann, pp. 33-50.
Yang, K.-H., Song, J.-K., Song, K.-I., 2013. Assessment of CO2 reduction of alkali-activated concrete. J. Clean. Prod. 39, 265-272.
Zhong, F., 2018. Is it time for China to switch to electric arc furnace steelmaking? (accessed 30/06/2020).

List of Tables

List of Figures